工学部SSSVプログラム
日中共同セミナー

（２０１２年３月５日―３月６日）

Research on self-mixing interference in fiber lasers and its applications

Ming Wang
School of Physical Science and Technology, Nanjing Normal University, No. 1 Wenyuan Road, Nanjing, Jiangsu 210046, China

ABSTRACT

In this paper, theory of self-mixing interference (SMI) in fiber ring lasers (FRLs) is analyzed. The theoretical model of vibration measurement based on SMI is designed. The relationship between vibration parameters and SMI signal is deduced. Experiment system is demonstrated and experimental results are compared with theoretical results. Theoretical model of self-mixing speckle effect (SMSE) in FRLs is analyzed. According to this theory, a model for velocity measurement is designed. The theory shows that the faster the velocity is, the more similar to Gaussian form the probability density distribution is. A method based on the fractal boxes of a section of speckle waveform is adopted for demodulation. The relationship between the numbers of boxes and velocities of the object is linear. Dual-channel SMI is presented demonstrating the potential for multiplexing in FRLs. The dual wavelengths of the FRL are selected by two fiber Bragg gratings (FBGs). The output power of dual-channel with optical feedback is theoretically deduced and simulated. The output variation and modes competition between the two channels in a fiber laser is also analyzed. The experimental results show a good agreement with the simulation, and indicate that SMI with parallel dual-channel is an efficient approach for multiple displacement measurement.

Self-Mixing Interference with sinusoidal phase modulation technique and its application for displacement sensing

Wei Xia and Ming Wang
Department of Physics Science and Technology, Nanjing Normal University
Wenyuan Road 1, Nanjing, 210046, China

1. Introduction

Self-mixing interference(SMI) phenomenon has been widely researched for the past decades, notably for displacement sensing [1]. SMI in a He-Ne laser has already been theoretically and experimentally demonstrated[2], and was used to measure displacement with an accuracy of $\lambda/2$ by counting the number of interference signal peaks. In order to improve the resolution of displacement measurement, a novel self-mixing interferometry based on sinusoidal phase modulating technique is proposed in this report. An electro-optic modulator(EOM) is situated in the external cavity of the laser to yield sinusoidal phase modulation of the interference signal. Moreover, the self-mixing interference signal is processed in frequency-domain to retrieve the vibration waveform of an object with an accuracy of tens of nanometer.

2. Experimental setup and results

The experimental setup is shown in Fig. 1, the light source is a linear polarized He-Ne laser. The beam emitted from the front mirror of the laser is sent through a variable attenuator, an EOM(New Focus, 4002), and then reflected back to the laser cavity by the external object(Corner Cube 2). The variable attenuator helps to assure that the self-mixing interferometry is running in the weak feedback regime. Therefore, the SMI signal is very close to a standard sinusoidal form. The EOM can provide pure phase modulation with extremely low amplitude modulation, when the polarization direction of the laser is parallel to the principal axis of the electro-optic crystal. The external object is fixed on a high-precision commercial PZT(PI P762.2l) which can obtain displacement accuracy of 1nm. The interference signal is monitored by a photodiode(PD) situated behind the back mirror of the laser. The electric output of PD is fed through low-pass filter, amplifier and data acquisition card. Hence, the digital signal is processed by a computer for reconstruction the vibration waveform of the object.

A calibration system is included in the experimental setup to evaluate the performance of the self-mixing interferometry. Orthogonal polarized dual-frequency laser emitted from the calibrator head(Agilent 5529A) is projected on the polarization beam splitter(PBS). One part of the laser with polarization direction perpendicular to the paper is reflected by PBS and corner-cube 1 and then collected by the detector of the calibrator head. The other part of the laser with polarization direction parallel to the paper is sent through the PBS, reflected by corner-cube 2 and then collected by the detector of the calibrator head as well. Combining the collected light, the calibrator provides a reference displacement for evaluating the performance of the proposed interferometry.

Firstly, PZT is controlled to vibrate at a sinusoidal form with fixed frequency of 10Hz. A set of reconstructed vibration waveforms at different amplitudes from 200 nm to 1000 nm are shown in the Fig. 2. In displacement measurement, only the relative value of two positions is important. So, only peak-to-peak amplitude is examined and the maximum error between the measured peak-to-peak amplitude of the vibration and reference peak-to-peak amplitude is less than 20nm.

Secondly, a instant start-up of a 2D-PZT movement has been tested. In Fig. 3(a), the dotted curve is the reconstructed vibration waveform by SMI and the solid curve is the reference vibration by Agilent 5529A. And the measurement result obtained by SMI is in good accordance with reference vibration. Simultaneous error between the two vibration waveforms is shown in Fig. 3(b) and the maximum displacement error is better than 20nm.

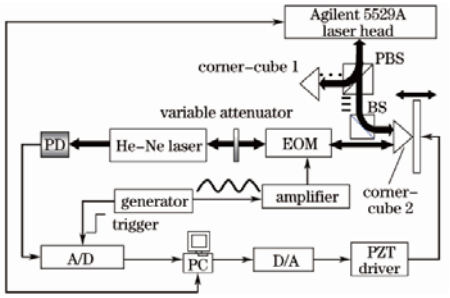

Fig.1 Experimental setup of self-mixing interferometry for displacement measurement.

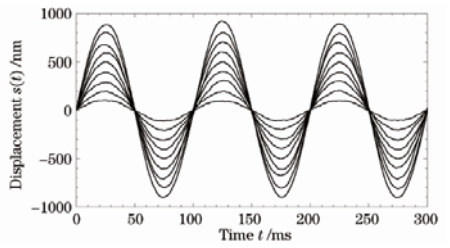

Fig.2 Reconstructed vibration waveforms of commercial PZT at different amplitudes.

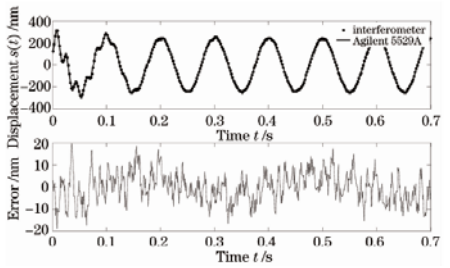

Fig.3 A measurement result of PZT from an instant start-up to steady state vibration. (a) Result comparison between SMI and calibrator; (b) Error.

3. Conclusion

An entire evaluation of the performance of self-mixing interferometry with sinusoidal phase modulation is firstly demonstrated. Experimental vibration measurement results of a commercial PZT are compared with simultaneous measurement results provided by Agilent 5529A and an accuracy of 20nm is achieved. It is shown that the phase-modulated laser self-mixing interferometer is suitable for real-time continuous vibration measurement on an accuracy of tens of nanometer.

References

[1]U. Zabit, et al., Opt. Lett., **35,** 8 (2010).
[2]S. Merlo, et al., IEEE J. Quantum Electron., 33**,** 4 (1997).

Sol-Gel co-assembly of hollow cylindrical inverse opals

Ni Haibin, Wang Ming and Chen Wei
Jiangsu Key Laboratory on Opto-Electronic Technology,
Department of Physics and Technology, Nanjing Normal University, Nanjing 210046, China

1. Introduction

Photonic band gap fibers (PBGFs) with hollow core guiding structures are a kind of microstructure optical fibers (MOFs) to overcome the limitations of traditional silica optical fibers [1]. Two dimensional photonic crystal fibers have been commercially available and widely used as sensing detectors, high power optical waveguides and nonlinear optical devices. Three dimensional (3D) PBGFs were proposed subsequently as its unique structure enables various applications in optical sensing and signal processing. It is challenging to fabricate silica air core cylindrical inverse opal fibers or waveguides both for template fabricating and infiltration materials to realize inverse opal structure. Recently Hatton et al. developed a sol-gel co-assembly method to overcome these difficulties [2]. We applied this method to producing inverse opals on capillaries' inner wall.

2. Experimental setup and results

Glass capillaries in 1.8mm, 850μm, 670μm diameters and in 10cm length were selected as an ideal cylindrical substrate. Aqueous plain PS microspheres solution with solids content ~10 wt. % was bought from Bangs Laboratories, Inc, and was only diluted to a certain concentration without any other treatment before use. The surface of the PS microspheres was covered with negatively-charged sulfate groups. Monodispersity of the PS microspheres is less than 10%. Capillaries were cleaned in an ultrasonic bath first using acetone and then deionized (DI) water for 10 minutes respectively. Then cleaned capillaries were dried with nitrogen before use. To fabricate HCIOs on the internal surface of capillaries, PS colloidal/TEOS solution dispersed in DI water with concentration of ~1vol % (PS spheres) and ~2vol % (TEOS solution [2]) was injected into a capillary. The height of the solution inside the capillary is 10-95mm and can be precisely controlled by a micro-pump. Length of the HCIOs was affected by the height of the inside solution. One end of the capillary was sealed to control the evaporation direction of solvent.

Silica inverse opals fabricated on a capillary's internal wall are with good quality, as seen in Fig.1. Fig.1 (a), (b), (c) exhibit optical microscope images observed in reflection mode: (a) a bare capillary, (b) a capillary with PS-silica gel CCC coated on its internal wall and (c) the capillary with silica inverse opals preserved on the internal wall after sintering. The axial uniformity together with the symmetric color distribution on the capillary internal edges attests to the high quality of the silica HCIO, which spectrally shifts the stop band with the viewing angle around the capillary curved surface. The color on the internal edge of the capillary has a blue shift after removing the PS colloidal crystal template as the effective refraction index decreased, as seen in Fig.1 (b) and (c). Fig.1 (d) ~ (g) are SEM images of the longitudinal-section of the capillary in (c). Image (d) is a top view at low magnification and (e) is longitudinal cross section of the silica inverse opals on the edge of the capillary internal wall with 7 layers. The robust inverse opals on the capillary internal wall are with good connectivity with the capillary substrate. Image (f) and (g) are curved surface of the HCIO with increased magnification. High uniform and ordered structure and small pores connected the big pores which reveal good connectivity of the structure can be observed. Fig.1 (h) and (i) show the top view of the cross section of a capillary with silica inverse opals coated on its internal wall. The internal diameter of capillaries could range from ~100μm to several millimeters as the ratio PS diameter to capillary diameter is very large. The average pore size of the fabricated inverse opals are 615nm, 500nm and 430nm, which made from PS spheres in 490nm, 580nm and 690nm diameters, with a contraction of 12.2%, 13.8% and10.8%, respectively.

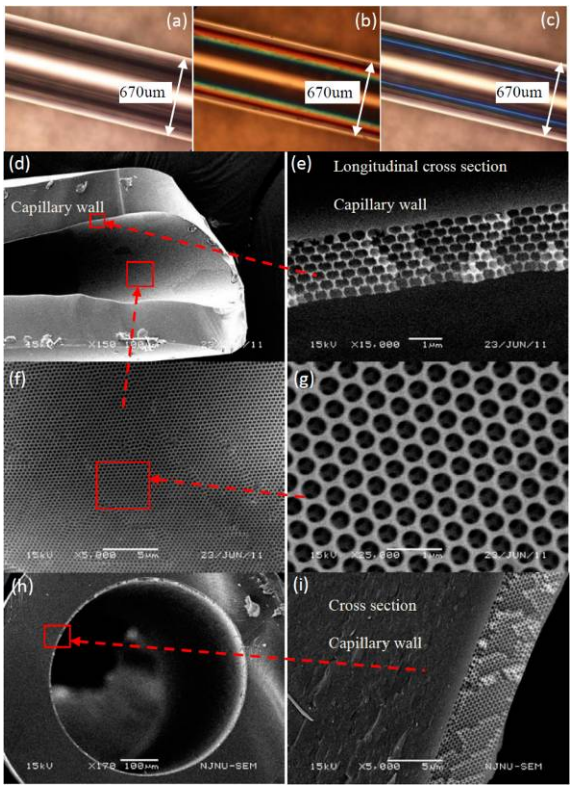

Fig.1. (a) ~ (c) are optical microscope images of capillaries in 350μm internal diameter. (a) bare capillary, (b) internal wall coated with composite colloidal crystal, (c) internal wall preserved with silica inverse opals after sintering. (d) ~ (i) are SEM images of inverse opals on the internal wall of a capillary, (d) longitudinal section of the capillary whose internal wall was coated with silica inverse opals, (e) longitudinal cross section of inverse opals, (f)surface of the inverse opals on the internal curved wall, (g) high magnification of the surface in (f), (h) and (i) are cross section of a capillary with silica inverse opals on its internal wall.

3. Conclusion

An approach of fabricating hollow cylindrical inverse opals by sol-gel co-assembly method was proposed. PS colloidal suspension added with hydrolyzed silicate precursor solution was used to vertical self-assemble composite colloidal crystals which consist of PS colloidal crystal template and infiltrated silica gel. Continuous silica hollow cylindrical inverse opal films have been produced on capillaries' inner surface.

References

[1]J. Li, et al., Opt. Express, **13** 17 (2005)
[2]B. Hatton, et al., P. Natl. Acad. Sci. USA, **107** 10354 (2010).

The Simulation of a Novel SU-8 Fiber Fabry-Perot Pressure Sensor

Lihua Dai and Ming Wang
Jiangsu Key Lab of Opto-electronic Technology , School of Physical Science and Technology,
Nanjing Normal University, Nanjing 210046, China

1. Introduction

With the fast evolving MicroElectroMechanical Systems (MEMS) technology, researchers are in more and more urgent need of improvement in the structure, fabrication or packaging of these Microsystems. The introduction of optics provides an opportunity to extend the use of these sensors to harsh environments. SU-8 photoresist is a kind of near UV photosensitive epoxy-based polymer. The molecular composition of this epoxy negative photoresist enables to produce uniform coatings. This high contrast photoresist has been used extensively in micromachining and other microelectronic applications, where a thick, chemically, and thermally stable image is desired, with an aspect ratio larger than 1:10.

2. Simulation and optimizations

The major difference between the proposed micro sensor and a traditional one is that the F-P sensor is designed for sensing lateral displacement instead of vertical one. The direction of F-P cavity change and the direction of exerting pressure are always the same in most reported sensors. Because of the F-P cavity length is microscale, the same direction could limit the range of the sensor's linear measurement. If it is overloaded, the membrane's deformation would get large enough to reach the other surface of F-P cavity, the sensor will out of order or, even worse, cause irreparable damage to itself. However, to make sure of the single-valued relation between deformation and the phase of interferential beam within the bandwidth of the light source, the cavity length should be small enough to keep the free spectrum range inside a little bit bigger than the working range. In this design, the directions of sensing membrane deformation from pressure and the change of cavity length are separated into two relative parts to meet requirements above perfectly.

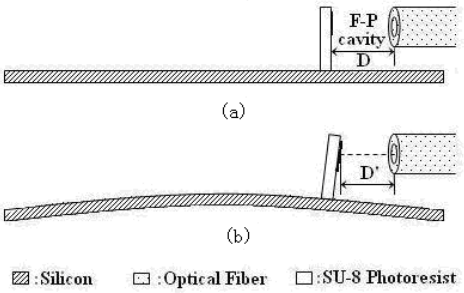

Fig.1. Schematic description of the micro Fabry-Perot sensor.

On account of the structure involving a connected movement, the deformation under load cannot be easily figured out through the existing formula. The behaviors of the sensor proposed can only be calculated by numerical simulation. The whole simulation is carried out by using commercial software CoventorWare.

Considering the stress concentration in all the corners, the circular membrane is selected as the fundamental shape of silicon diaphragm.

Fig.3 is demonstrated that there is a certain position where the square column be placed to acquire a maximum value of lateral displacement under a constant pressure. A conclusion can be drawn from Fig.4 that the dimension of the square column doesn't impact the lateral displacement a lot. The shift of peak value is only because of the size of contact area, which affects the deformation of the diaphragm and the angle of tilt of the column.

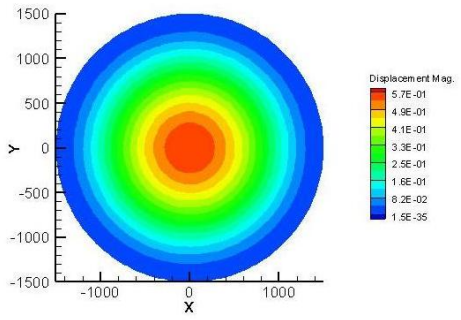

Fig.2. The distribution of the deformation.

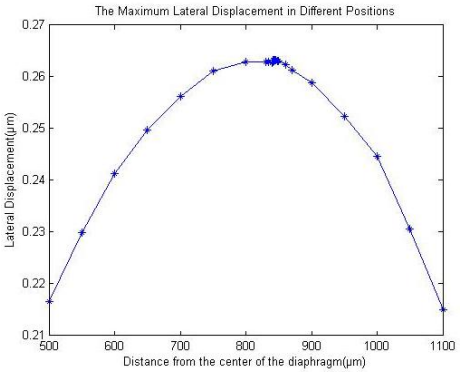

Fig.3. Relationship between the position of the square column and the attainable maximal lateral displacement.

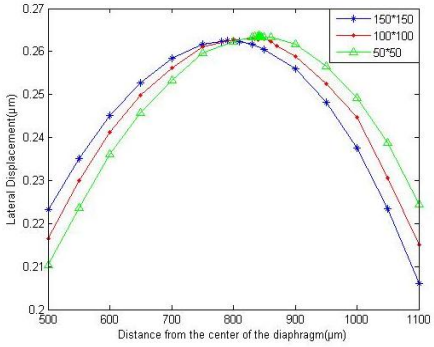

Fig.4. The Comparison of different design dimensions.

3. Conclusion

The novel design broadedens the range of linear measurement of pressure sensors. The sensitivity is 2.606μm/Mpa by simulation. The characteristic result here verifies the feasibility of the design. Through numerical simulations, we further confirm and optimize the parameters of the structure. The accurate micro-pressure detection is widely needed in industrial field. The excellent characters make the perspective more wide.

References

[1]Y.Ge, et al., Sensors and Actuators A: Physical, **143,** 224 (2007).
[2] I. Pardon, et al., Sensors Journal, **11,** 343 (2011).
[3] C. J. Lin, et al., Sensors and Actuators A: Physical, **113**, 12 (2004).

High channel-count ultra-narrow comb-filter based on a sampled fiber Bragg grating

Hongpu Li and Xuxing Chen
Department of Electrical and Electronic Engineering, Shizuoka University,
3-5-1, Johoku, Hamamatsu, 432-8561, Japan
dhli@ipc.shizuoka.ac.jp

Abstract An ultra-narrow comb-filter formed by a piezoelectric transducer (PZT)-induced phase-shift in a phase-only sampled FBG is proposed and experimentally demonstrated. Moreover, the high channel-count scheme based on a triply sampled FBG is firstly proposed.

1. Introduction

The high channel-count comb filters with ultra-narrow bandwidth have attracted lots of interesting in the fields such as the wavelength selection, multiwavelength fiber laser and RF single generation[1-2]. The multi-channel ultra-narrow filter can easily be realized by introducing a phase shift into a sampled fiber Bragg grating (FBG). To date, several kinds of Multi-channel FBG have been proposed and demonstrated, such as the sinc-sampled FBG, the superimposed FBG, the Talbot-effect based FBG and the amplitude-phase sampled FBG. In particular, the phase-only sampled FBG, a special case of the amplitude-phase sampled FBG, has the advantages of high channel counts, minimum index-modulation, high uniformity of inter-channel, and compatibility with the standard of international telecommunications union (ITU) grids. In this study, a PZT-induced phase shift in a linearly chirped 51-channel FBG is firstly demonstrated and a comb filter with 51-channel is thus successfully obtained. Moreover, based on a sampled FBG with simultaneous utilization of two amplitude-assisted phase sampling (AAPS) functions and a phase-only sampling (POS) function, a comb filter with consecutive 1377 channels enabling to cover whole band of (O+E+S+C+L+U) is numerically demonstrated, which has a channel-bandwidth of 1.5 GHz and channel spacing of 25 GHz.

2. Realization of comb filter based on a phase-shift 51-chanel phase-only sampled FBG

Principle of the proposed comb-filter is schematically shown in Fig. 1(a). The comb filter with ultra-narrow bandwidth can be obtained by utilizing two phase-only sampled 51-channel gratings which have identical characteristics. The gratings are particularly designed with channel spacing of 0.8 nm exactly fitted with the ITU channel grids. The grating strength is about 10 dB with a length of about 12 cm and the flat-top bandwidth for each channel is about 0.6 nm. One of the gratings is working in the transmission with π phase-shift introduced by a PZT which is wholly glued to the grating. The other (without the glued PZT) is placed in a temperature chamber and working in the reflection. Fig. 1(b) shows the measured 5-channel transmission spectrum for these two cascaded FBGs (the voltage applied on the PZT is 150 V) where the inset shows the whole spectrum coving 51-channel. It can be seen that multichannel band-pass filter has been obtained and each of the channel has almost the same characteristics with a bandwidth of about 0.027 nm.

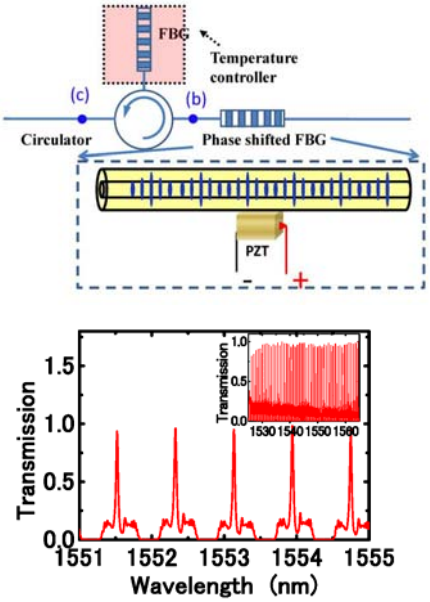

Fig. 1. (a) Setup for the realization of the proposed comb-filter and (b) transmission spectrum for the two cascaded multi-channel FBGs.

3. High channel-count Comb-filter based on a triply sampled FBG

Most recently, we have reported a doubly sampling approach enabling to create an ultrahigh-channel-count FBG with both high channel uniformity and high in-band energy efficiency [2]. In this study, a triple sampling method is firstly proposed for the design of a FBG-based comb-filter. Unlike the previous doubly-sampling scheme, here the sampling function adopted is a typical one consisting of three sampling functions which can be expressed as

$$S(z) = S_{a1}(z) \cdot S_{a2}(z) \cdot S_{p3}(z), \quad (1)$$

where Sa1(z) and Sa2(z) both are the pre-optimized amplitude-assisted phase-only sampling (AAPS) functions. Each of them has small in-band channels of $(2N_1+1)$ and $(2N_2+1)$, respectively. Meanwhile $S_{p3}(z)$ is a pre-optimized phase-only sampling (POS) function with a relative larger number of in-band channels $(2N_3+1)$. Figure 2 shows the principle of the triply sampled FBG based on the Fourier analysis. The detailed processes can be summarized as follows. Step 1: As a seed grating, a single channel FBG with ultra-narrow bandwidth is firstly designed by using the transfer matrix method (TMM); Step 2: By utilizing the simulated annealing method and the Gerchberg-Saxton algorithm, optimizations for the three sampling functions are accomplished. A $(2N_1+1)$ channel FBG can be generated in the frequency domain by multiplying the function S_{a1} with the seed grating in spatial domain, which could be seen in Fig. 2(b). Step 3: In the spatial domain, the second amplitude-assisted phase sampling function S_{a2} is then multiplied by the originated $(2N_1+1)$ channel FBG, then in the frequency domain, an FBG with $(2N_1+1)(2N_2+1)$ channels could be obtained as is shown in Fig. 2(c). Note that, to avoid overlapping between the generated channels, the condition $P_2 \le P_1/(2N_1+1)$ should be satisfied. Step 4: The phase-only sampling function $S_{p3}(z)$ with a higher channel-count of $2N_3+1$ is then multiplied by the two amplitude-assisted phase-only sampled FBG as is shown Fig. 2(d). To avoid overlapping between the generated channels, the condition $P_3 \le P_2/(2N_2+1)$ should be satisfied. Figure 2(e) shows the reflection spectrum of the realized FBG using the triple sampling method, it can be seen that one can easily obtain consecutive $(2N_1+1)(2N_2+1)(2N_3+1)$ channels with channel spacing of $\Delta\nu_1 = c/2n_{eff}P_1$ in the frequency domain as long as the conditions $P_2=P_1/(2N_1+1)$ and $P_3=P_2/(2N_2+1)$ are satisfied.

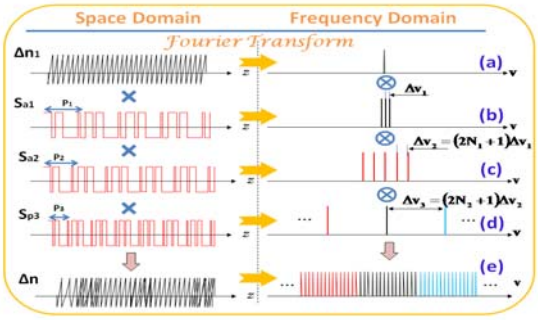

Fig. 2. Fourier analysis of the proposed triple sampling method for the FBG based comb filter.

To verify the above proposals, design for a FBG with 1377 channels is implemented. Firstly, two AAPS functions with 3-, 9-channel and a POS function with 51-channel are optimally designed. Secondly, a seed grating is designed by using the TMM method. The seed grating is designed to have a narrow bandwidth of 1.5 GHz. By multiplying the seed grating with the 3-, 9- and 51-channel sampling functions simultaneously in spatial domain, an ultrahigh channel-count FBG with 51 sets of 3x9 channels can be obtained. Figure 3 shows the designed results for the spectrum of the comb filter, where high uniform 1377-channel with a narrow bandwidth of 1.5 GHz is successfully obtained.

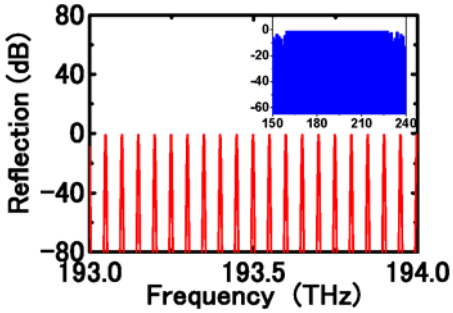

Fig. 3. Design results for a 1377-channel comb filter with spacing of 25 GHz. The inset show the whole spectra one.

4. Conclusions

In this study, a comb filter with 51-channel is experimentally demonstrated. Moreover, based on the triple sampling method, a FBG based filter having a bandwidth@3-dB of 1.5 GHz, channel spacing of 25 GHz, and a consecutive 1377 channel is numerically demonstrated.

5. References

[1] M. Ibsen et al, IEEE Photon. Tech. Lett. 10, 842 (1998).

[2] H. Li et al, Opt. Lett. 34, 938 (2009).

Fabrication of a phase-shifted long-period fiber grating by using CO_2 laser

CO_2 レーザによる 位相シフト長周期ファイバグレーティングの作製

Keisuke Hishiki　Taki Yosuke　Goto Yuji　Lunlun Xian　Hongpu Li
日紫喜 圭介　瀧　洋丞　後藤 祐志　線　倫々　李　洪譜
Faculty of Engineering, Shizuoka University
静岡大学　工学部

1. Introduction

In the past decades, long-period fiber gratings (LFG) have been widely studied and found many applications in the fields of optical communications and optical sensing system, such as the band-rejection filter, gain-spectrum flattening filter, temperature and refractometric sensors, etc. Recently, the phase-shifted LFG has attracted a progressive interest due to its potential applications being able used as an optical differentiator and a sub-picosecond pulse shaper [1-2]. In this study, a simple approach to write LFG and create a typical phase-shift in the LFG have been proposed and firstly demonstrated, which is based on the thermal shock effect realized by using a high frequency CO_2 laser pulses.

2. Fabrication setup

Figure 1 shows the experimental setup, which consists of a CO_2 laser controlling system, a beam moving and a focusing system, a fiber alignment stage, and a in-line system to measure the transmission spectrum of the fabricated LFG, where the utilized fiber is single-mode one provided by Fujikura Inc (FutureGuide®-SR15E), the CO_2 laser (SYNRAD-20, emission at the central wavelength of 10.2 μm) works at a typical frequency of 5 kHz with a duty-cycle changeable form %1 to 99%. For the grating fabrication, the aligned CO_2 laser beam is focused through a ZnSe lens with a focus length of 70 cm. The minimum spot size (CO_2 laser) on the fiber is ～100 μm, which makes the focusing laser mainly absorbed by the fiber in a very short time, and thus makes a permanent index-change within the exposure region of the fiber core based on the thermal shock effect. Period of the fabricated LFG is precisely controlled by periodically moving the motored stage (including the reflection mirror) and turning on/off the laser shutter through the LabView controlling software. For the measurement, an amplified spontaneous emission (ASE) source and an optical spectral analyzer (OSA) are utilized to measure the transmission spectrum of the LFG in the real time.

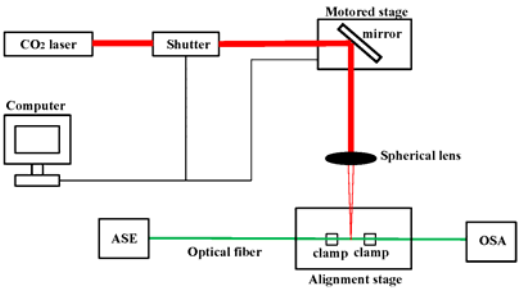

Fig. 1. Fabrication setup for the long-period fiber grating.

3. Experimental results and discussions

At first, we fabricated a couple of long-period gratings, while the average power of the CO_2 laser is kept in 5 W. The gratings are continuously written with number of 46 period and each period adopted is ～650 μm. Figure 2 shows the transmission spectrum of a typical grating, from which it can be seen that the typical characteristic of LFG is really realized. There exist a resonant attention peak located at a wavelength between 1540 and 1560 nm, which can be attributed to the strong coupling between the forward core-mode and one of cladding-modes (LP_{15} mode in our case). It is also seen that the resonant attention is larger than 25dB, giving that the coupling efficient κ combined with the grating length L is given to be $\kappa L \approx 0.482\pi$. Furthermore, we measure the transversal profile of the written LFG by using an atomic force microscopy (AFM), no any damages and defects have been found, which in return means that the large index-change in the core is caused by the change of the densification and the residual stress of the fiber core through the thermal shock effect [2].

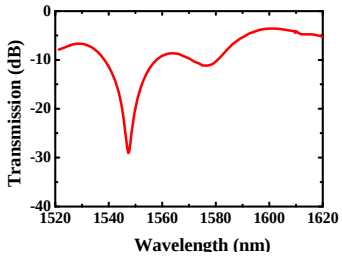

Fig. 2. Transmission spectrum of LPG without phase shift.

Secondly, we also wrote several phase-shifted LFGs by using the same setup as shown in Fig. 1, where the inserted phase-shift are realized by purposely change the local period of the moving stage. In our case, a π phase shift is assumed to be inserted at middle of the grating. In order to realize it, we simply change the moving period of motored-stage from 650 μm to 325 μm just for the period at middle of the grating (i.e., the 23th period in our case). Figure 3 shows the measurement result for a typical phase-shifted grating, from which it can be seen that the LP_{15} peak shown in Fig. 2 is split into two, which agrees well with the theoretical one what the Ref [3] expects.

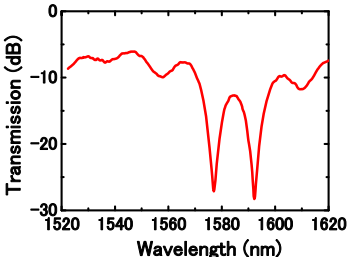

Fig. 3. Transmission spectrum of LPG with a phase shift.

4. Conclusions

A simple approach based on the utilization of a high-frequency CO_2 laser has been proposed and successfully demonstrated for the fabrication of both a LFG and a phase-shifted LFG. This kind of devices may provide potential applications to fiber optical sensor and all-optical signal processing.

References

[1] Y. J. Rao, et al., Opt. Communications, **229**, 209 (2004).
[2] R. Slavik, et al., Opt. Express, **14** , 10699 (2006).
[3] H. Ke et al., IEEE Photon. Techn. Lett. **19**, 1596 (1998).

Enhanced Slow Light in a Phase-Shifted Multichannel Fiber Bragg Grating Assisted by Stimulated Brillouin Scattering

Lunlun Xian[1] and Hongpu Li[2]
[1]Graduate School of Science and Technology, [2]Department of Electrical and Electronic Engineering, Faculty of Engineering, Shizuoka University, Johoku 3-5-1, Hamamatsu, 432-8561, Japan

1. Introduction

Slow light has found many applications such as optical buffering, high-resolution interferometers etc. Slow light in single channel fiber Bragg grating (FBG) has already been theoretically and experimentally demonstrated [1]. However, to date there is no demonstration of slow light in a multichannel FBG. On the other hands, stimulated Brillouin scattering (SBS) is another important method to realize a tunable slow light in optical fibers [2]. In this report, a multichannel slow-light is firstly demonstrated in a piezoelectric transducer (PZT)-induced phase-shifted multichannel FBG. The group delay is controlled by applying different voltages on the PZT. Moreover, the group delay in each channel can be further enhanced by incorporating SBS.

2. Experimental setup and results

The experimental setup is shown in Fig. 1, where the input signal is generated by externally modulating a tunable distributed-feedback (DFB) laser (LD1: with a linewidth of 20 MHz) through a $LiNbO_3$ amplitude modulator (LM), which is driven by a sinusoid signal with a frequency of 450 MHz. The resulted pulses are amplified by an Erbium doped fiber amplifier (EDFA 1) and transmit through a phase-shifted multichannel FBG. The FBG is a phase-only sampled 51-channel FBG [3] possessing a channel spacing of 0.8 nm, a grating strength of about 10 dB, a length of about 12 cm and a flat-top bandwidth for each channel of about 0.6 nm. The phase shift is induced by a PZT attached to the grating at the central position [3]. To monitor the notch wavelength of the phase-shifted FBG which determines the wavelength selection of LD1, an amplified spontaneous emission (ASE) source incorporated with a circulator CL2, a 3-dB coupler (CPLR), and an optical spectrum analyzer (OSA) are utilized. Moreover, an optical isolator (OI1) is used to isolate the light reflected by the grating and the isolator OI2 is used to isolate the Brillouin pump light. Note that the output signal from the phase-shifted FBG is used as Brillouin probe signal. To realize SBS amplification, another tunable DFB laser (LD2: with a linewidth of 100 kHz) is used as the SBS pumping source amplified by an amplifier (EDFA 2). In addition, a 500-m high-nonlinear fiber (HNLF) is used as Brillouin gain medium. The signal after the circulator CL1 is detected by a fast photodiode (PD) which is connected to a sampling oscilloscope (OSC) or a RF spectrum analyzer (RFSA).

First, only the phase-shift multichannel FBG is used for slow light while the SBS is not employed. The wavelength of LD1 is tuned to 1550.4 nm as reference (Ref) as shown in Fig. 2. The signal transmitted through the FBG is recorded by OSC. Then the wavelength of LD1 is tuned to notch wavelength of 1549.932 nm in channel #1. Two voltages of 40 V and 90 V are in turn applied on PZT to control the phase shift. The transmitted signals for the two cases are recorded by OSC. Comparing with Ref, the delay times are 0.041 ns and 0.06 ns for 40 V and 90 V, respectively. To verify multichannel operation, the wavelength of LD1 is then tuned to 1550.739 nm in #2. The measurement of the transmitted signal is repeated. Comparing with Ref, the delay times with #2 are 0.031 ns and 0.076 ns for 40 V and 90 V, respectively. Next, SBS is employed to further increase the group-delay within any individual channel. For convenient, channel #1 is only selected for the test. The voltage applied on the PZT is 90 V. By carefully tuning the wavelength of LD2, the amplification due to the SBS can be clearly verified by the RFSA. Figure 3 shows the recorded output waveforms. Compared with above results, it is obviously seen that the group delay is further enhanced from 0.06 to 1.473 ns at Brillouin pump power of 50 mW.

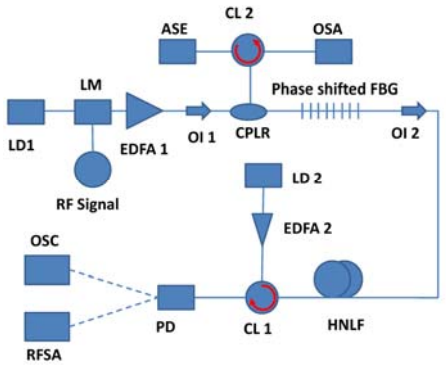

Fig.1. Experimental setup for the slow-light measurement.

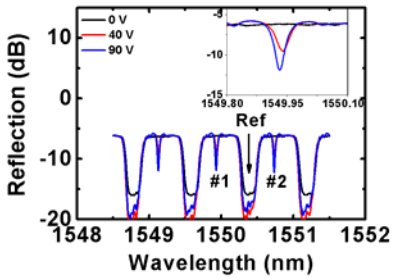

Fig.2. Measured reflection spectrum with different voltages on the PZT. Inset shows notches in #1.

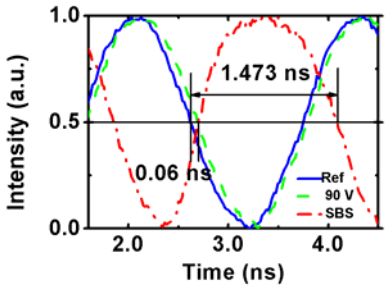

Fig.3. Measurement results for the output waveforms assisted with SBS.

3. Conclusion

Slow light utilizing a PZT-induced phase-shift multichannel FBG is firstly demonstrated in experiment. The group-delay can be tuned by adjusting the voltage on the PZT. The delayed time in each channel can be further enhanced by incorporating SBS.

References

[1]S. Longhi, et al., Electron. Lett., **41,** 1075 (2005).
[2]K. Song, et al., Opt. Express, **13,** 82 (2004).
[3]X. Chen, et al., Photon. Technol. Lett.. **23**, 498 (2011).